RSC Advances

PAPER

View Article Online
View Journal | View Issue

Cite this: *RSC Adv.*, 2017, **7**, 26776

Insights into the role of the interface defects density and the bandgap of the back surface field for efficient p-type silicon heterojunction solar cells†

Fengyou Wang,[a] Yanbo Gao,[a] Zhenyu Pang,[abc] Lili Yang*[a] and Jinghai Yang*[a]

Received 9th April 2017
Accepted 14th May 2017

DOI: 10.1039/c7ra04018k

rsc.li/rsc-advances

An n-type silicon wafer appears to be an excellent base material for high efficiency silicon heterojunction solar cells with high annual energy output. The further development of viable p-wafer cells would open many industrial photovoltaic options. Here, the role of the interface defects density and the bandgap of the back surface field of p-type silicon heterojunction solar cells have been investigated in detail to provide guidelines for achieving high performance. The result indicates that the output characteristics of the heterojunction solar cells are sensitive to the density of interface defects (D_{it}) at both sides of the c-Si surface. However, the output parameters primarily affected by D_{it} at the front and rear side are not identical. Back surface field (BSF), which aims to reduce photo-generated carriers' recombination at the rear interface, has also been optimized by adjusting the bandgap to improve the collection efficiency. Finally, based on experimental results, we propose that the conversion efficiency of p-type silicon heterojunction solar cells could be increased beyond 23% by efficiently regulating the bifacial D_{it} and the bandgap of the BSF layer.

1. Introduction

Silicon heterojunction (SHJ) solar cells constructed with ultra-thin hydrogenated amorphous silicon (a-Si:H) on a crystalline silicon (c-Si) absorber layer are promising candidates for high-efficiency, low-cost solar cells. Compared with traditional monocrystalline silicon solar cells, SHJ solar cells generally exhibit higher open-circuit voltages (V_{oc}) because wide-bandgap a-Si:H is used as the emitter layer and the metal contact is separated from the wafer by a-Si:H films and indium tin oxide (ITO), which reduces the amount of interface recombination.[1–3] Moreover, SHJ solar cells could be fabricated with low-temperature or photolithographic-free processes, since passivation of the c-Si wafer surfaces and formation of the emitter and back surface field (BSF) are all performed with thin intrinsic and doped a-Si:H layers, usually deposited by low-temperature plasma-enhanced chemical vapor deposition.[4,5]

So far, the highest efficiency silicon heterojunction solar cells were obtained using n-doped, rather than p-doped, c-Si wafers.[6] However, n-type wafers are still less readily available on the market than p-type wafers, which are widely used for the production of conventional (diffused-emitter) silicon solar cells. The possibility to produce high-efficiency heterojunction solar cells from p-type wafers is, thus, of great practical interest. The p-type SHJ solar cells have already been demonstrated by several groups but with efficiencies significantly lower than those achieved on n-type wafers.[3,5,6] For p-type silicon heterojunction solar cells, the performance is also more sensitive to the density of a-Si:H/c-Si interface defects, not only because the p–n junction is across two different materials, but also owing to the asymmetry between the conduction and valence band offsets.[7] Yet up to now, there still have unified understanding about the different influences caused by the D_{it} at the front and rear sides of the p-type SHJ solar cells. Thus, it is necessary to understand the role of the D_{it} and the bandgap alignment for p-type SHJ solar cells in order to further improve the performance and accelerating its practical application.

Numerical analysis describe the basic phenomena present in photovoltaic devices, allowing intuitive examination of each parameter in solar cells and thus identifying the optimal conditions for operating. In this work, we make an insight into the relationship of the D_{it} at the front and rear sides of the crystalline silicon by an extended Shockley–Read–Hall formalism.[8] Our results present that the D_{it} at front side is primarily affected the V_{oc} of the p-type SHJ solar cells, while the D_{it} at the rear side could act upon the FF and J_{sc} of the device.

[a]Key Laboratory of Functional Materials Physics and Chemistry of the Ministry of Education, Jilin Normal University, Siping 136000, China. E-mail: yanglili1998@126.com; jhyang1@jlnu.edu.cn

[b]Changchun Institute of Optics, Fine Mechanics and Physics, Chinese Academy of Sciences, Changchun 130033, China

[c]University of the Chinese Academy of Sciences, Beijing 100049, China

† Electronic supplementary information (ESI) available. See DOI: 10.1039/c7ra04018k

Also, in order to achieve a good function of photo-generated carriers' collection, the bandgap of the BSF should be adjusted in the range of 1.7–1.8 eV to achieve the efficiency more than 23%.

2. Numerical modeling

In order to give an accurately insight into the sensitive parameters for p-type SHJ solar cells, analytical calculations are unavoidable tool to model the behavior of a full cell architecture especially under equilibrium conditions. The Poisson and the continuity equations for electrons and holes are solved considering Shockley–Read–Hall recombination statistics for the a-Si:H and for the defect layer at the interface between a-Si:H and c-Si. In practical manufacturing process, D_{it} can be suppressed by wet chemical cleaning of the c-Si surface followed by H-terminated and the growth of a-Si:H, which saturates the silicon dangling bonds with atomic hydrogen.[9–11] Garín *et al.*[12] suggested that the Shockley–Read–Hall formalism, which has been widely used to depict c-Si surface passivation schemes by SiO_2 and a-SiN_x:H, can model the i-a-Si:H/c-Si interface recombination, in which the i-a-Si:H thin film dangling bond states in the proximity of abrupt i-a-Si:H/c-Si interface can be considered to be an effective interface and included in D_{it}. Nevertheless, the charge effect of doped a-Si:H layer defects on the interface recombination was eliminated, and D_{it} was oversimplified by a single level defect state at mid-gap. Shu *et al.*[13] extend the Shockley–Read–Hall approach to more accurately model the interface recombination through a continuously distributed D_{it}, with the effect of doped a-Si:H defect states also taken into account. Herein, we further extend this comprehensive Shockley–Read–Hall model in this work by inducing a defect layer to describe injection level dependent surface recombination velocity (S_{it}).

The complete architecture of ITO/n-a-Si:H/i-a-Si:H/p-c-Si/i-a-Si:H/p^+-a-Si:H/Ag and corresponding bandgap schematic diagram in this numerical analysis are exhibited in Fig. 1a and b. We performed numerical simulations of p-type SHJ solar cells with efficient tool named AFORS-HET.[14] The basic parameters in this numerical modeling, which extract from different state-of-the-art SHJ solar cells experimental results,[6,15–18] are shown as Table 1. The absorber of the solar cell is standard 300 μm thick p-type c-Si, with an acceptor density of 1.5×10^{16} cm^{-3}. It is characterized by a single donor-type defect centered at mid-gap with a density of 10^{10} cm^{-3} and the capture cross section for holes and for electrons is equal to 10^{-14} cm^2. The density of states of the n-a-Si:H emitter layer and i-a-Si:H passivation layer, including two Gaussian distributions of deep defects and the valence and conduction band tails states are exhibited in Fig. 1c and d. An 80 nm ITO is used to be the transparent conductive oxide layer and a thin c-Si layer (3 nm) with average distribution continuous donor and acceptor defect states in the band gap has been inserted between the i-a-Si:H and c-Si to substitute the interface defects. The density of interface defects translates into a volume defects density by:

$$d \times S \times \rho_{volume} = S \times \rho_{interface} \quad (1)$$

where d is the thickness of the volume defects layer, S is the surface area of the c-Si, ρ_{volume} and $\rho_{interface}$ are the defect states density at the volume and surface of c-Si respectively. The surface recombination velocities of the electrons and holes are both set to 1.0×10^7 cm s^{-1}. The solar AM1.5 radiations are adopted as the illuminating source with the power density of 100 mW cm^{-2} and the ITO/n-a-Si:H contact is fixed as flat band in calculations.

3. Results and discussion

Role of the bifacial D_{it} for p-type SHJ solar cells

Recombination through defect levels in semiconductors is usually described by the Shockley–Read–Hall theory in this work. The surface recombination rate (N_s) of solar cells can be given by,[19]

$$N_s = \frac{\left(n_s p_s - {n_i}^2\right) v_{th} D_{it}}{\left(\frac{n_s + n_1}{\sigma_p} + \frac{p_s + p_1}{\sigma_n}\right)} \quad (2)$$

Where σ_n, σ_p and n_s, p_s are the capture cross-sections and concentrations of electrons and holes respectively. v_{th} is the thermal velocity. n_1 and p_1 are the statistical factor for electrons and holes respectively. Therefore, the S_{it} could be given as,

$$S_{it}(\Delta n) = \frac{N_s}{\Delta n} = \frac{\left(n_s p_s - {n_i}^2\right) v_{th}}{\Delta n} \int_{E_v}^{E_c} \frac{D_{it}(E)}{\left(\frac{n_s + n_1}{\sigma_p} + \frac{p_s + p_1}{\sigma_n}\right)} dE \quad (3)$$

where Δn_s is the excess carrier density at the surface. For SHJ solar cells, the V_{oc} is related to the interface recombination *via*:[20]

$$V_{oc} = \frac{\phi_B}{q} - \frac{nkT}{q} \ln\left(\frac{qN_V S_{it}}{J_{SC}}\right) \quad (4)$$

kT is the thermal energy, ϕ_B is the effective barrier, q is the elementary charge, N_v is the effective density of states in the valence band. According to eqn (3) and (4), it can be concluded that $(n_s p_s - {n_i}^2)$ and D_{it} affect the performance of the solar cells by determining the V_{oc}. So we assumed different D_{it} at the front side of c-Si surface to depict the corresponding influences on device, thus providing the threshold of the D_{it} to maintain high performance p-type SHJ solar cells.

Fig. 2a shows the band diagrams with different values of D_{it} at the front side of the heterojunction under illumination. The interface charge (Q_{it}) by trapping carrier is related to D_{it} (E) and the difference in occupancy by electrons and holes *via*[13]

$$Q_{it} = -q \int_{E_v}^{E_c} D_{it}^{A}(E) f_A(E) dE + q \int_{E_v}^{E_c} D_{it}^{D}(E) f_D(E) dE \quad (5)$$

where the $D_{it}^{A}(E)$ and $D_{it}^{D}(E)$ are the continuous distributed acceptor-type and donor-type $D_{it}(E)$ within c-Si bandgap. The $f_D(E)$ and $f_A(E)$ are the occupancies of the donor and acceptor defects states, respectively, expressed by

$$f_A(E) = \frac{n_s \sigma_n + p_1 \sigma_p}{(n_s + n_1)\sigma_n + (p_s + p_1)\sigma_p} \quad (6)$$

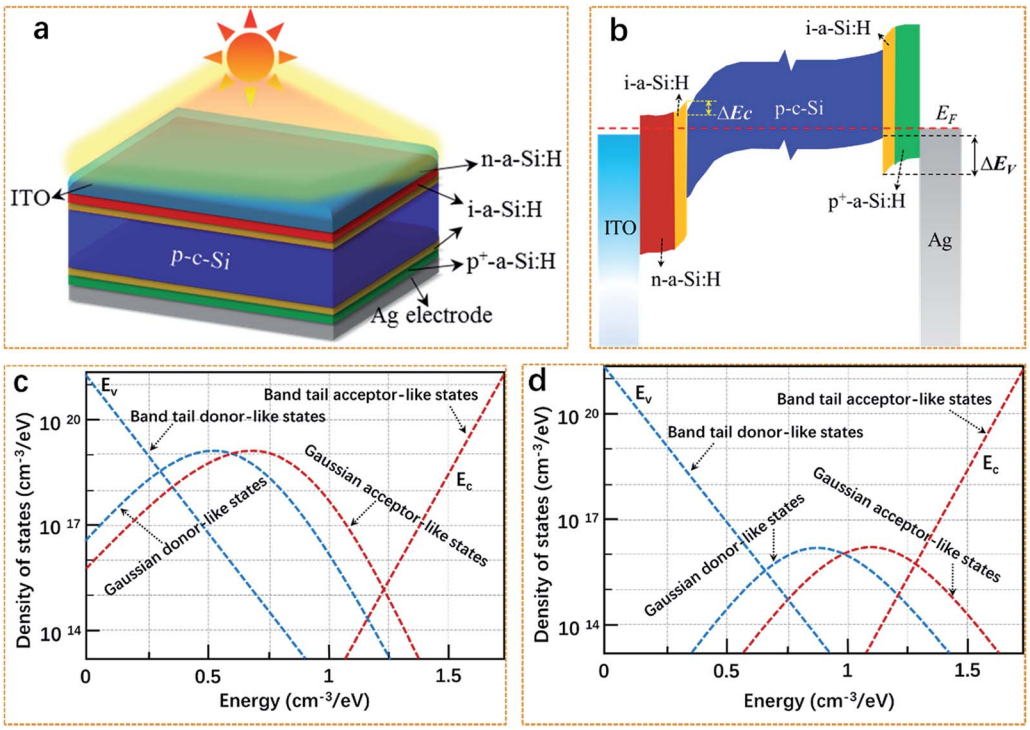

Fig. 1 (a) Schematic of the SHJ solar cells for numerical analysis. (b) Schematics of energy diagram of p-type SHJ solar cell at equilibrium condition. The dashed lines are Fermi energy (E_F), conduction band offset (ΔE_c) and valence band offset (ΔE_v), respectively. Distribution of gap defects in (c) n-a-Si:H and (d) i-a-Si:H layer include two Gaussian distributions of deep defects and the band tails states of the valence band and conduction band.

$$f_D(E) = \frac{n_1\sigma_n + p_s\sigma_p}{(n_s + n_1)\sigma_n + (p_s + p_1)\sigma_p} \quad (7)$$

Since the minority carriers in p-type are electrons, which have larger capture cross sections than holes, the high D_{it} will increase the number of Q_{it} by trapping carriers. If Q_{it} can become comparable with the charges in the a-Si:H and c-Si, and hence the bands need to realign to keep the system charge balance.[21] As a result, the band bending (ψ) in c-Si is reduced (ψ_1, ψ_2, and ψ_3 are the equilibrium band bending in c-Si when the D_{it} are 10^9, 10^{12}, and 10^{13} cm^{-2} eV^{-1}, respectively). Meanwhile, the recombination possibility at the a-Si:H/c-Si heterointerface will increase with the reduction of the band bending, due to the declining of the driven force in c-Si for separating photo-generated carriers.[22]

The influences of D_{it} on the rear-side heterojunction band bending have been exhibited in Fig. 2b. As described above, the number of trapped holes will be much larger than that of electrons, and thus creating positively Q_{it}. Similar with the front side, when the magnitude of Q_{it} can be closed to the ionized donor in the depletion region (*e.g.*, 10^{13} cm^{-2} eV^{-1}), c-Si energy band at rear interface even can bend downward. Fig. 2c shows that the photo-generated holes and electrons current density (J_n and J_p) as a function of position in the p-type SHJ solar cells

Table 1 Main parameter values adopted for SHJ solar cells in this study

Parameters	a-Si:H(n)	a-Si:H(i)	a-Si:H(p$^+$)	c-Si(p)
Layer thickness (nm)	10 nm	5 nm	5 nm	300 μm
Electron affinity (eV)	3.9	3.9	2.9	4.05
Mobility gap (eV)	1.80	1.80	Variable	1.12
Optical band gap (eV)	1.72	1.72	1.72	1.12
Effective density of states N_c/N_v (cm^{-3})	$10^{20}/10^{20}$	$10^{20}/10^{20}$	$10^{20}/10^{20}$	$2.8 \times 10^{19}/2.6 \times 10^{19}$
Doping concentration (cm^{-3})	5×10^{20}	$N_d = 100$	9×10^{20}	1.5×10^{16}
Electron mobility (cm^2 V^{-1} s)	5	5	5	1041
Hole mobility (cm^2 V^{-1} s)	1	1	1	412.9
Standard deviation in Gaussian states (eV)	0.21	0.21	0.21	—
Electron capture cross (cm^2)	7×10^{-16}	7×10^{-16}	3×10^{-15}	1×10^{-14}
Hole capture cross (cm^2)	7×10^{-16}	7×10^{-16}	3×10^{-14}	1×10^{-14}
Urbach energies $E_{tail,V}$ and $E_{tail,C}$ (eV)	0.094/0.068	0.094/0.035	0.12/0.08	—

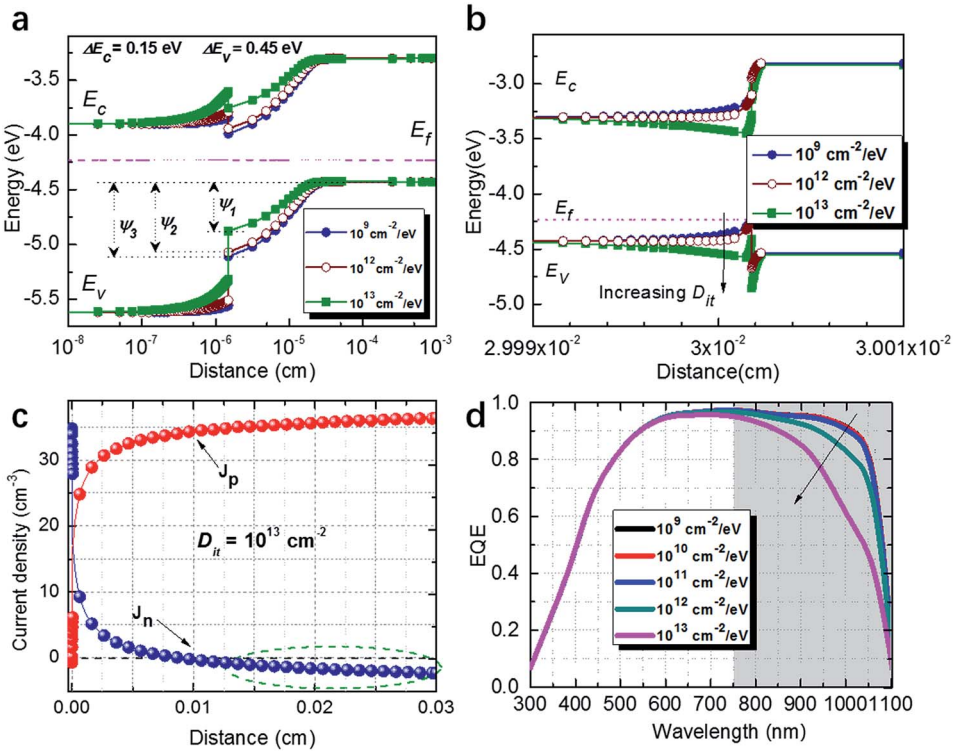

Fig. 2 Band diagrams and quasi-Fermi levels of the heterojunction in (a) front and (b) rear side of the p-type SHJ solar cells as the D_{it} increased from 10^9 cm^{-2} eV^{-1} to 10^{13} cm^{-2} eV^{-1}. ψ_1, ψ_2, and ψ_3 are the equilibrium band bending in c-Si when the D_{it} is 10^9, 10^{12}, and 10^{13} cm^{-2} eV^{-1}, respectively. (c) The photo-generated holes and electrons current density (J_n and J_p) as a function of position in the SHJ solar cells when the D_{it} at rear side is 10^{13}cm^{-2} eV^{-1}. (d) The EQE spectrum of the p-type SHJ solar cells with different D_{it} at rear side of c-Si.

when the D_{it} of the rear hetero-interface is 10^{13} cm^{-2} eV^{-1}. The negative partial of J_n (circled in green dash) means the opposite diffused electrons from the front side of c-Si to the rear side of it owing to the band bend downward.[23] Apparently, the negative J_n is controversial to the operating electron current of the solar cells, and will increase the recombination probability with the majority carries (holes) at the rear p-c-Si/p$^+$-a-Si:H interface. Fig. 2d shows the external quantum efficiency (EQE) spectrum of the solar cells. The response at long wavelength has obviously decreased when D_{it} increased to 10^{13} cm^{-2} eV^{-1}, which is accordance with the opinion that the recombination at rear c-Si/a-Si:H interface become more seriously.

Fig. 3 shows the cells' performances as a function of the D_{it} at front and rear sides of the c-Si, respectively. Fig. 3a shows that V_{oc} significantly decreases about 300 mV as the D_{it} at the front i-a-Si:H/p-c-Si interface increases from 10^9 cm^{-2} eV^{-1} to 10^{13} cm^{-2} eV^{-1} because of the increased interface recombination. While the V_{oc} is not seriously affected as the increasing D_{it} of the rear side. However, it could be found that the fill factor (FF), short-circuit current density (J_{sc}), and conversion efficiency (Eff) have been seriously decreased when the D_{it} of the rear side increase to 10^{13} cm^{-2} eV^{-1}.

The reason for this phenomenon could be ascribed to the relation between the D_{it} and the trapped charges at hetero-interface. As concluded from eqn (3) and (4), the D_{it} could directly impact on the V_{oc} of the solar cells by changing band bending the recombination velocity of the front-side hetero-interface. Compared with the influences of front D_{it} on the device, the D_{it} of rear side has relatively small impact on the V_{oc}. As most of the photons are absorbed at the front side of c-Si, the entire photo-generated carriers are separated (and transporting)

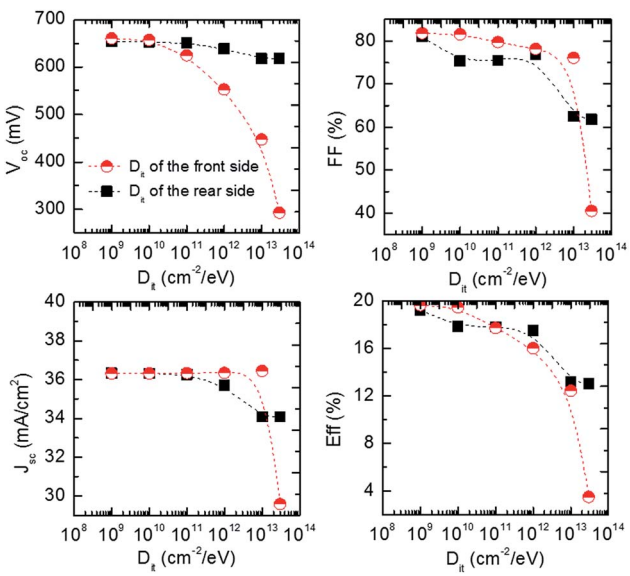

Fig. 3 The V_{oc}, J_{sc}, FF and Eff of p-type solar cells as functions of the D_{it} at the front side and rear side of the solar cells.

basically rely on the built-in field established by front n-a-Si:H and p-type c-Si.[24,25] Heterojunction established at the rear side is not the decisive factor for the V_{oc} of the cells. The main function of the p$^+$-a-Si:H BSF is to enhance carriers' selective holes-collection and transportation. Hence, the changed energy band structure of the rear p-c-Si/p$^+$-a-Si:H junction has a relatively small impact on V_{oc} compare with the one of n-a-Si:H/p-c-Si junction. However, the FF and J_{sc} are more sensitive to the rear-side D_{it} because of the band bending downward, which caused by high D_{it} (as shown in Fig. 2b), could induce the opposite electron current and creating a barrier for majority carrier (holes) transportation, thus increasing the series resistance of the p-type SHJ solar cells.

Analytical BSF's bandgap of p-type SHJ solar cells

The BSF layer should be included to obtain good cell performance. The offsets of the conduction band and valence band at heterojunction are:

$$\Delta E_c = \chi_{c\text{-}Si} - \chi_{a\text{-}Si:H} \quad (8)$$

$$\Delta E_v = E_{g_{a\text{-}Si:H}} - \chi_{c\text{-}Si} + \chi_{a\text{-}Si:H} - E_{g_{c\text{-}Si}} \quad (9)$$

where $\chi_{c\text{-}Si}$, $\chi_{a\text{-}Si:H}$, $E_{g_{c\text{-}Si}}$ and $E_{g_{a\text{-}Si:H}}$ are the electron affinity and bandgap of c-Si and a-Si:H. The electron affinity of c-Si and a-Si:H is 4.05 eV and 3.9 eV, respectively. In practical experiment, the bandgap of the BSF could be adjusted by changing certain parameters of the p$^+$-a-Si:H layer, such as the hydrogen content, doping concentration and crystallization.[26,27] Fig. 4 shows the performance of the p-type SHJ solar cells as a function of BSF's bandgap. The V_{oc} of the solar cells is improved significantly as the bandgap increased from 1.2 to 1.9 eV. The J_{sc} and FF of the solar cells are almost unaffected with the increasing of the bandgap of the BSF below 1.8 eV. While a pronounced decreasing could be found for J_{sc} and FF if further increasing the bandgap of the BSF to 1.9 eV.

The band diagrams of the rear side p-c-Si/p$^+$-a-Si:H structure are shown in Fig. 5, considering the BSF bandgap of 1.3 eV and 1.8 eV, respectively. The wide bandgap (1.8 eV) of BSF with a large conduction band offset could achieve good surface field for the rear-side diffusing electrons of the device.[26–28] However, the valence band offset also increased, and hence establishing a large barrier for holes to flow through the rear contact. However, in contrast, the low bandgap of the BSF layer resulted in band bend downward and small conduction band offset. As illustrated for Fig. 2b, this is detrimental for electrons diffused forward and will increase the recombination possibility at rear surface.

Fig. 6 shows the EQE variation with bandgap to further explain the previously described results. With the bandgap increased from 1.3 to 1.72 eV, the spectrum response at longer wavelengths increased due to the suppressing of the recombination, which caused by enhancing back surface field effect. However, further increasing the bandgap will decrease the spectrum response owing to the large valence band offset blocking the majority holes' transportation. Thus, it can be concluded that there exists a trade-off between surface field effect and carrier transportation barrier, and it could be relaxed by carefully regulating the bandgap of the BSF layer. Also, the numerical calculation results indicate that the optimum bandgap of BSF should be controlled in the range of 1.7 to 1.8 eV for p-type SHJ solar cells in practical processing.

Finally, as shown in Fig. 7, when the defect states density at both side of the c-Si is 10^{10} cm^{-2} eV^{-1}, and the bandgap of the BSF layer is 1.72 eV (the thickness of a-Si:H emitter layer and intrinsic layer is set as 5 nm and 3 nm respectively. The doping concentration of n-a-Si:H and p$^+$-a-Si:H layers are 6×10^{21} cm^{-3} and 9×10^{19} cm^{-3} respectively), an efficiency of the 23.27% could be achieved. The performance of the solar cells as a function of the c-Si thickness has also been study, which has been shown in Fig. S1 and S2.† It should be noted that this results are obtained only based on planar p-type substrate without incorporating any antireflection coating and light trapping architecture. Hence, for p-type SHJ solar cells, a more than 24% efficiency could be expected with fully designed light-

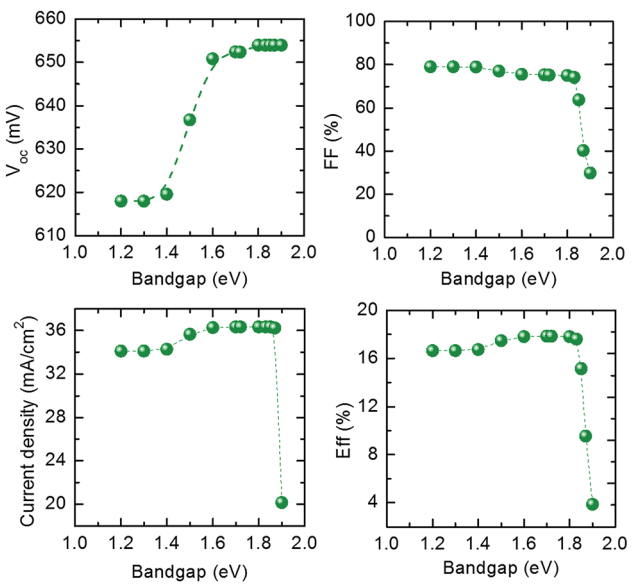

Fig. 4 The V_{oc}, J_{sc}, FF and Eff of p-type solar cells as functions of the BSF's bandgap.

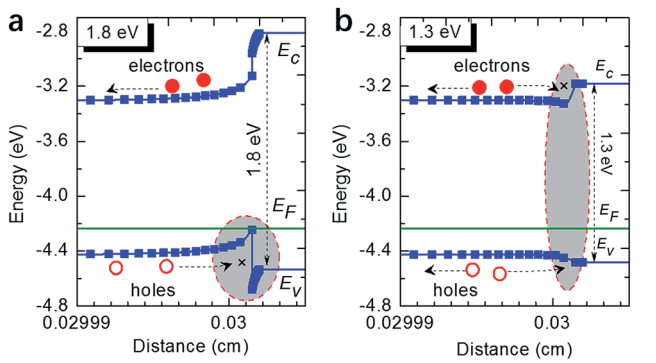

Fig. 5 Band diagrams of the rear-side heterojunction when the bandgap of the BSFs are (a) 1.8 eV and (b) 1.3 eV, respectively.

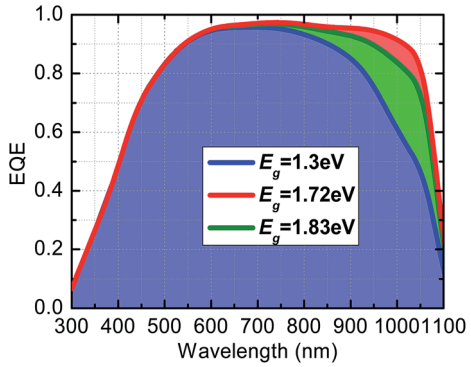

Fig. 6 The EQE curves of the p-type SHJ solar cells when the bandgap of the BSF layers variant from 1.3 eV to 1.8 eV.

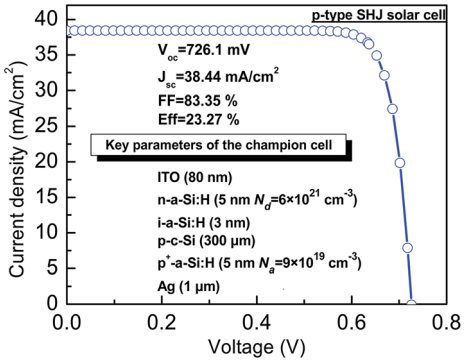

Fig. 7 Illuminated current density–voltage curve of the champion cell. All the optimized parameters are extracted from the practical experimental results.

management strategies in practical application. Based on the performance and cost analysis, it is observed that besides n-type solar cells, the simple and low-cost p-type SHJ solar cells with optimized D_{it} and BSF layer may also be potential candidate for high efficiency solar cell technology.

4. Conclusions

In summary, the influence of interface defects at both side of c-Si and bandgap of BSF layer on p-type SHJ solar cell performance were investigated though numerical calculations. Hence, suggestive design parameters for p-type SHJ solar cell fabrication are proposed. The result shows that D_{it} at front and rear side of c-Si should be controlled lower than 10^{13} cm^{-3} to avoid significantly negative impact on the solar cells performance. Meanwhile, D_{it} at front side directly determine the values of V_{oc}. While D_{it} at the rear side of the solar cell seriously affects the J_{sc} and FF. Appropriate designation for the bandgap of the BSF (1.7–1.8 eV) can improve the efficiency of the p-type SHJ solar cells by relaxing the trade-off between surface field effect and carrier transportation barrier. Finally, a conversion efficiency of more than 23% could be achieved by adopting the parameters extracted from experimental results. This highlights that SHJ solar cells based on low-cost p-type c-Si may also be the market-leading products owing to the improvements on cost-to-performance ratio for c-Si photovoltaics.

Acknowledgements

The authors gratefully acknowledge the support from National Nature Science Foundation of China (Grant No. 61475063, 61505067 and 21576111), Program for New Century Excellent Talents in University (No. NCET-13-0824).

References

1 Y. Jia, J. Wei, K. Wang, A. Cao, Q. Shu, X. Gui, Y. Zhu, D. Zhuang, G. Zhang, B. Ma, L. Wang, W. Liu, Z. Wang, J. Luo and D. Wu, *Adv. Mater.*, 2008, **20**, 4594–4598.
2 Y. Jia, A. Cao, X. Bai, Z. Li, L. Zhang, N. Guo, J. Wei, K. Wang, H. Zhu, D. Wu and P. M. Ajayan, *Nano Lett.*, 2011, **11**, 1901–1905.
3 M. Lu, S. Bowden, U. Das and R. Birkmire, *Appl. Phys. Lett.*, 2007, **91**, 063507.
4 Y. Liu, J. Zhang, H. Wu, W. Cui, R. Wang, K. Ding, S.-T. Lee and B. Sun, *Nano Energy*, 2017, **34**, 257–263.
5 F. Wang, R. Du, Q. Ren, C. Wei, Y. Zhao and X. Zhang, *J. Mater. Chem. C*, 2017, **5**, 1751–1757.
6 K. Yoshikawa, H. Kawasaki, W. Yoshida, T. Irie, K. Konishi, K. Nakano, T. Uto, D. Adachi, M. Kanematsu, H. Uzu and K. Yamamoto, *Nat. Energy*, 2017, **2**, 17032.
7 D. Macdonald and A. Cuevas, *Phys. Rev. B: Condens. Matter Mater. Phys.*, 2003, **67**, 075203.
8 N. Jensen, U. Rau, R. M. Hausner, S. Uppal, L. Oberbeck, R. B. Bergmann and J. H. Werner, *J. Appl. Phys.*, 2000, **87**, 2639–2645.
9 G. D. Cody, T. Tiedje, B. Abeles, B. Brooks and Y. Goldstein, *Phys. Rev. Lett.*, 1981, **47**, 1480–1483.
10 A. A. Langford, M. L. Fleet, B. P. Nelson, W. A. Lanford and N. Maley, *Phys. Rev. B: Condens. Matter Mater. Phys.*, 1992, **45**, 13367–13377.
11 P. Biswas, D. Paudel, R. Atta-Fynn, D. A. Drabold and S. R. Elliott, *Phys. Rev. Appl.*, 2017, **7**, 024013.
12 M. Garín, U. Rau, W. Brendle, I. Martín and R. Alcubilla, *J. Appl. Phys.*, 2005, **98**, 093711.
13 Z. Shu, U. Das, J. Allen, R. Birkmire and S. Hegedus, *Progress in Photovoltaics: Research and Applications*, 2015, **23**, 78–93.
14 M. Schmidt, L. Korte, A. Laades, R. Stangl, C. Schubert, H. Angermann, E. Conrad and K. V. Maydell, *Thin Solid Films*, 2007, **515**, 7475–7480.
15 S. Avasthi, S. Lee, Y.-L. Loo and J. C. Sturm, *Adv. Mater.*, 2011, **23**, 5762–5766.
16 M. Smeets, K. Bittkau, F. Lentz, A. Richter, K. Ding, R. Carius, U. Rau and U. W. Paetzold, *Nanoscale*, 2016, **8**, 18726–18733.
17 M. Agarwal, A. Pawar, N. Wadibhasme and R. Dusane, *Sol. Energy*, 2017, **144**, 417–423.
18 J. Yu, J. Bian, W. Duan, Y. Liu, J. Shi, F. Meng and Z. Liu, *Sol. Energy Mater. Sol. Cells*, 2016, **144**, 359–363.

19 S. Olibet, E. Vallat-Sauvain, L. Fesquet, C. Monachon, A. Hessler-Wyser, J. Damon-Lacoste, S. De Wolf and C. Ballif, *Phys. Status Solidi A*, 2010, **207**, 651–656.
20 M. Mikolášek, J. Racko and L. Harmatha, *Appl. Surf. Sci.*, 2017, **395**, 166–171.
21 R. Hussein, D. Borchert, G. Grabosch and W. R. Fahrner, *Sol. Energy Mater. Sol. Cells*, 2001, **69**, 123–129.
22 S.-C. Shiu, J.-J. Chao, S.-C. Hung, C.-L. Yeh and C.-F. Lin, *Chem. Mater.*, 2010, **22**, 3108–3113.
23 Y. Zhang, C. Yu, M. Yang, Y. He, L. Zhang, J. Zhang, X. Xu, Y. Zhang, X. Song and H. Yan, *RSC Adv.*, 2017, **7**, 9258–9263.
24 L. Mazzarella, S. Kolb, S. Kirner, S. Calnan, L. Korte, B. Stannowski, B. Rech and R. Schlatmann, in *2016 IEEE 43rd Photovoltaic Specialists Conference (PVSC)*, 2016, pp. 2955–2959.
25 K. Ding, X. Zhang, F. Xia, R. Wang, Y. Kuang, S. Duhm, J. Jie and X. Zhang, *J. Mater. Chem. A*, 2017, **5**, 285–291.
26 M. H. Brodsky, M. Cardona and J. J. Cuomo, *Phys. Rev. B: Condens. Matter Mater. Phys.*, 1977, **16**, 3556–3571.
27 J. Kakalios, R. A. Street and W. B. Jackson, *Phys. Rev. Lett.*, 1987, **59**, 1037–1040.
28 L. Zhao, G. Wang, H. Diao and W. Wang, *Phys. Status Solidi RRL*, 2016, **10**, 730–734.